Journal of Engineering Mathematics (2024) 146:4
https://doi.org/10.1007/s10665-024-10355-1

A novel asymptotically consistent approximation for integral evaporation from a spherical cap droplet

Alexander W. Wray[1] · **Madeleine R. Moore**[2]

Received: 23 October 2023 / Accepted: 28 February 2024

Abstract
The total evaporation rate due to a volatile capillarity-dominated droplet diffusively evaporating into the surrounding gas is a critically important quantity in industrial and engineering applications such as Q/OLED screen manufacturing. However, the analytical expression in terms of integrals in toroidal coordinates can be unwieldy in applications, as well as expensive to compute. Therefore, simple yet highly accurate approximate solutions are frequently used in practical settings. Herein we present a new approximate form that is both accurate and fast to compute, but also retains the correct asymptotic behaviour in the key physical regimes, namely hydrophilic and superhydrophobic substrates, and a hemispherical droplet. We illustrate this by comparison to several previous approximations and, in particular, illustrate its use in calculating droplet lifetimes, as well as approximating the local evaporative flux.

Keywords Approximate solutions · Capacitance · Droplets · Evaporation

1 Introduction

In this short note, we consider the problem of a droplet of volatile fluid that evaporates into the surrounding vapour. The liquid has density $\tilde{\rho}$ and vapour–liquid surface tension coefficient $\tilde{\gamma}$, where both are taken to be constant. The droplet is assumed to be axisymmetric, with contact radius and contact angle given by $\tilde{R}$ and θ_c, respectively. The droplet is assumed to be sufficiently small that the effects of gravity are negligible

✉ Alexander W. Wray
alexander.wray@strath.ac.uk

Madeleine R. Moore
m.r.moore@hull.ac.uk

[1] Department of Mathematics and Statistics, University of Strathclyde, Livingstone Tower, 26 Richmond Street, Glasgow G1 1XH, UK

[2] Department of Mathematics, University of Hull, Cottingham Road, Hull HU6 7RX, UK

Published online: 17 April 2024

compared to capillarity, so that the Bond number $\mathrm{Bo} = \tilde{\rho}\tilde{g}\tilde{R}^2/\tilde{\gamma} \ll 1$, where g is the magnitude of acceleration due to gravity.

We assume that the droplet is evaporating in the diffusion-limited regime [1, 2], and that the droplet is sufficiently small that the effects of convection in the atmosphere may be neglected. Typically, this restricts us to sub-millimetric droplets, although there is some variation depending on the liquid and vapour properties (see [3–5] for a fuller discussion). Moreover, we shall assume that the timescale for the droplet to fully evaporate is sufficiently slow compared to the rate at which vapour diffuses away from the interface that we may model the evaporative process as quasi-steady: these conditions are met widely for many different liquid, vapour and substrate combinations (see, for example, [1, 2] for a discussion). In particular, this assumption combined with the dominance of capillarity in the droplet leads to the droplet taking the form of a spherical cap throughout the evaporative process [6, 7].

For a spherical cap droplet with radius $\tilde{\mathcal{R}}$ resting on a flat substrate, we work relative to cylindrical polar coordinates $(\tilde{r}, \psi, \tilde{z})$, where the substrate is located at $\tilde{z} = 0$ so that $\tilde{r} = 0$ is the axis of the droplet. In this coordinate system, the droplet interface lies at $\tilde{z} = \tilde{h}$, where [8]

$$\tilde{h} = -\tilde{\mathcal{R}}\cos\theta_c - \sqrt{\tilde{\mathcal{R}}^2 - \tilde{r}^2}, \quad \text{where} \quad \tilde{\mathcal{R}} = \tilde{R}\operatorname{cosec}\theta_c. \tag{1}$$

The local evaporative flux $\tilde{J}$ is given by Fick's law as $\tilde{J} = -\tilde{D}\mathbf{n}\cdot\nabla\tilde{c}$, where $\mathbf{n}$ is the unit outward normal to the interface, $\tilde{D}$ is the diffusion coefficient, and $\tilde{c}$ is the vapour partial density in the atmosphere, which satisfies Laplace's equation, subject to $\tilde{c} = \tilde{c}_{\mathrm{sat}}$ on the droplet interface, where $\tilde{c}_{\mathrm{sat}}$ is the saturation concentration, $\partial\tilde{c}/\partial\tilde{z} = 0$ on the substrate, and $\tilde{c} \to \tilde{c}_\infty$ in the far field, where c_∞ is the ambient concentration. The focus of the present note is the integral flux $\tilde{F}$ from the surface of the droplet, defined by

$$\tilde{F} = \iint_\Sigma \tilde{J}\,\mathrm{d}S, \tag{2}$$

where Σ is the liquid free surface. Following [8], the system is non-dimensionalised according to

$$\tilde{\mathbf{x}} = \tilde{R}_0\mathbf{x}, \quad \tilde{R} = \tilde{R}_0 R, \quad \tilde{c} = \tilde{c}_\infty + (\tilde{c}_{\mathrm{sat}} - \tilde{c}_\infty)c, \quad \tilde{J} = \frac{\tilde{D}(\tilde{c}_{\mathrm{sat}} - \tilde{c}_\infty)}{\tilde{R}_0}J, \tag{3}$$

$$\tilde{F} = \tilde{D}(\tilde{c}_{\mathrm{sat}} - \tilde{c}_\infty)\tilde{R}_0 F, \quad \tilde{t} = \frac{\rho}{2\tilde{D}(\tilde{c}_{\mathrm{sat}} - \tilde{c}_\infty)}\left(\frac{3\tilde{V}_0}{2\pi}\right)^{2/3} t, \tag{4}$$

where $\tilde{t}$ denotes time, $\mathbf{x}$ denotes the usual spatial position, and $\tilde{R}_0$ and $\tilde{V}_0$ are the values of $\tilde{R}$ and the volume at the initial time $\tilde{t} = 0$.

The integral flux is a quantity of some importance. It dictates droplet lifetimes [9] which can be crucial in everything from vapour phase deposition control [10] to COVID risk [11], and is a necessary precursor to predicting other phenomena such as multi-droplet interactions [12, 13].

However, while the result for a flat droplet ($\theta_c \sim 0$) has been known since at least [14] ($F = 4R$), the result for spherical cap droplets (the default shape for small droplets where capillarity dominates) was not established until the works of [15], [7] and [1], who find that the integral flux is given by

$$\frac{F}{R} = \pi \left[\tan \frac{\theta_c}{2} + 8 \int_0^\infty \frac{\cosh^2 \theta_c \tau}{\sinh 2\pi \tau} \tanh((\pi - \theta_c)\tau) \, \mathrm{d}\tau \right]. \tag{5}$$

However, (5) relies on having access to a quick, accurate and reliable numerical integration package for practical implementation. Unfortunately, a commercial software license is not always readily available, and moreover, depending on the target use case, even then the calculation may be too slow for practical purposes. For example, modern ultra-high definition screens are manufactured using a printing process involving $O(10^8)$ pixels [16]. At this scale, speed of computation is crucial.

As a result, a variety of approximations have come to be used in engineering and practical applications. Picknett & Bexon [17] suggested

$$F_{\text{pick}} = \begin{cases} F_{\text{p,thin}}, & 0 \le \theta_c < 0.175, \\ F_{\text{p,thick}}, & 0.175 \le \theta_c \le \pi, \end{cases} \tag{6}$$

$$R^{-1} F_{\text{p,thin}} = \operatorname{cosec} \theta_c \left(4\theta_c + 0.60262\theta_c^2 - 0.386039\theta_c^3 \right), \tag{7}$$

$$\begin{aligned} R^{-1} F_{\text{p,thick}} = \operatorname{cosec} \theta_c \, (&0.000562785 + 3.97914\theta_c \\ &+ 0.728849\theta_c^2 - 0.557821\theta_c^3 + 0.0649053\theta_c^4 \Big), \end{aligned} \tag{8}$$

based on polynomial fitting to exact values of F (determined from an infinite series alternative to (5)). Bourges & Shanahan [18] used a simplified model of a droplet of spherical cap shape as in fact being a sphere to determine the approximation

$$R^{-1} F_{\text{bour}} = -2\pi \frac{\cot \theta_c}{\log(1 - \cos \theta_c)}, \tag{9}$$

while Hu & Larson [7] use a fitting to FEM calculations to yield

$$R^{-1} F_{\text{hula}} = \pi (1.30 + 0.27\theta_c^2). \tag{10}$$

Hu et al. [19] employed a model approximating a droplet of arbitrary contact angle as an equivalent droplet with the same surface area but contact angle $\theta_c = \pi/2$ to yield the estimate

$$R^{-1} F_{\text{huwu}} = \frac{2\pi}{\sqrt{1 + \cos \theta_c}}. \tag{11}$$

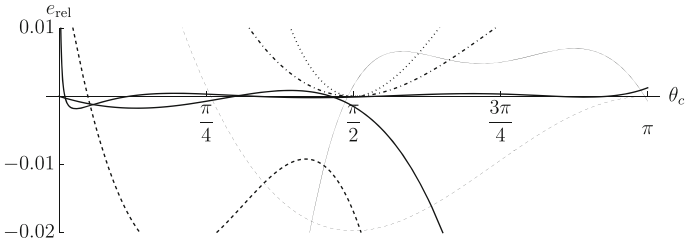

Fig. 1 The relative error in the integral flux compared to the exact solution (5) for $F_{\mathrm{p,thin}}$ and $F_{\mathrm{p,thick}}$ (8) (7) (thick, solid curves), F_{bour} (9) (dotted curve), F_{hula} (10) (thick, dashed curve), F_{huwu} (11) (dash-dotted curve), F_{bhar} (12) (thin curve) and F_{lest} (13) (thin dashed curve)

Bhardwaj [20] gave an approximation based again on matching to FEM, but using a more sophisticated ansatz, resulting in the formula

$$R^{-1}F_{\mathrm{bhar}} = \tan\frac{\theta_c}{2}\left(4.28 + 6.11\exp\left[-0.45\theta_c^2\right]\right). \tag{12}$$

Finally, Lebedev-Stepanov & Savenko [21] recently suggested the approximate form,

$$R^{-1}F_{\mathrm{lest}} = \frac{2\pi\log 2}{\cos(\theta_c/2)}. \tag{13}$$

These are compared with the exact solution (5) in Fig. 1. Note that they all suffer substantial deviations ($> 1\%$) in large portions of the domain, or deviate substantially at important points, where the asymptotic behaviour is well known (e.g. $\theta_c = 0^+, \pi/2, \pi^-$).

We give here a brief note resolving these issues for a variety of use cases. In Sect. 2, we discuss the asymptotic properties of the exact solution in three key scenarios and, in particular, illustrate the deficiencies of previous estimates in the thin-droplet limit, $\theta_c \to 0^+$. We construct our new approximation in Sect. 3 and compare it to existing models in Sect. 4. We then illustrate its effectiveness in the particular application of evaluating droplet lifetimes in Sect. 5.1, and for approximating the local flux in Sect. 5.2. We conclude with a summary and discussion in Sect. 6. Finally, we note that, except in Sect. 5.1, we take $R \equiv 1$.

2 Asymptotic properties of the integral flux

In this section, we consider three particular contact angles that are important in applications, namely a droplet on a superhydrophobic substrate ($\theta_c \to \pi^-$), a hemispherical droplet ($\theta_c \to \pi/2$) and a droplet on a hydrophilic substrate ($\theta_c \to 0^+$). Note that the final case may also be viewed as the thin-droplet limit frequently used in studies of topics such as particle deposition and the coffee ring effect in evaporating droplets (see, for example, [22] for a discussion of the thin-droplet limit).

Performing an asymptotic expansion of (5) in the superhydrophobic limit, we find that the integral flux has the asymptotic expansion

$$F = \frac{4\pi \log 2}{\pi - \theta_c} + O(\pi - \theta_c) \tag{14}$$

as $\pi - \theta_c \to 0^+$.

Similarly, when the contact angle is close to $\pi/2$, the expansion for the integral flux satisfies

$$F = 2\pi + \pi(\theta_c - \pi/2) + O((\theta_c - \pi/2)^2) \tag{15}$$

as $\theta_c - \pi/2 \to 0$.

Finally, we turn to the hydrophilic limit. In particular, expanding in θ_c inside the integral in (5) and integrating term-by-term suggests the expansion

$$F = \frac{4\pi}{\theta_c} \log\left(\frac{\pi}{\pi - \theta_c}\right) + \sum_{j=1}^{\infty} L(2j) \sum_{i=2j}^{\infty} (-i)_{2j-1} \left(\frac{\theta_c}{\pi}\right)^i \tag{16}$$

as $\theta_c \to 0^+$, where $(\cdot)_\alpha$ denotes the falling factorial;

$$L(j) = (-1)^{j/2}(2^{j-1} - 1)2^{5-2j} \frac{\zeta(j)^2}{\pi^j}; \tag{17}$$

and $\zeta(j)$ is the zeta function. The inner sum in (16) is

$$\sum_{i=2j}^{\infty} (-i)_{2j-1} \left(\frac{\theta_c}{\pi}\right)^i = \pi \left(\pi^{-2j}(\pi - \theta_c)^{2j} - 1\right)(\pi - \theta_c)^{-2j} \theta_c^{2j-1} \Gamma(2j) \tag{18}$$

as $\theta_c \to 0^+$, where $\Gamma(\alpha)$ is the Gamma function. Hence, for practical computational purposes, an approximation of the integral flux is given by truncating the series as

$$\begin{aligned} F = {} & \tfrac{4\pi}{\theta_c} \log\left(\tfrac{\pi}{\pi - \theta_c}\right) + \textstyle\sum_{j=1}^{N} (-1)^j (2^{2j-1} - 1) 2^{5-4j} \tfrac{\zeta(2j)^2}{\pi^{2j-1}} \\ & \times \left((1 - \theta_c/\pi)^{2j} - 1\right)(\pi - \theta_c)^{-2j} \theta_c^{2j-1} \Gamma(2j) \end{aligned} \tag{19}$$

as $\theta_c \to 0^+$. In particular, we note that

$$\begin{aligned} F = {} & 4 + \tfrac{2}{\pi}\theta_c + \left(\tfrac{1}{9} + \tfrac{4}{3\pi^2}\right)\theta_c^2 + \left(\tfrac{1}{\pi^3} + \tfrac{1}{6\pi}\right)\theta_c^3 \\ & + \left(-\tfrac{7}{2700} + \tfrac{4}{5\pi^4} + \tfrac{2}{9\pi^2}\right)\theta_c^4 + O\left(\theta_c^5\right) \end{aligned} \tag{20}$$

as $\theta_c \to 0^+$, which, at leading order, recovers the expected Weber result for a flat disk [14].

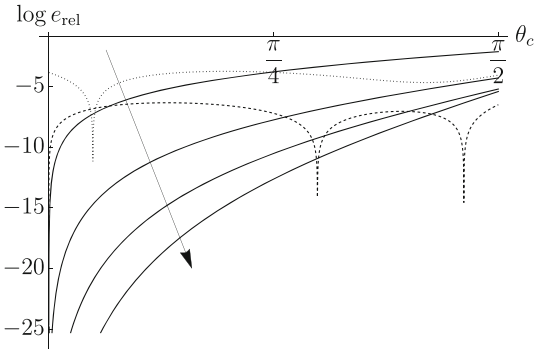

Fig. 2 Logarithmic relative error of different approximations to the exact solution (5). The two best previous approximations for thin droplets are displayed, namely $F_{\text{p,thin}}$ (7) (dashed curve) and F_{hula} (10) (dotted curve) alongside the first few truncations $N = 0, 1, 2, 3$ (solid curves) of the exact asymptotic solution as $\theta_c \to 0^+$. The arrow indicates direction of increasing N

As two representative approximations from the literature, $F_{\text{p,thin}}$ (7) and F_{hula} (10) are compared against appropriate truncations of (19) in Fig. 2 (note that other approximations discussed previously perform substantially worse in this hydrophilic limit). We see clear evidence that the previous approximations perform poorly as $\theta_c \to 0^+$, with relatively few terms of the truncated asymptotic series needed to outperform both for even moderately large values of θ_c.

3 Derivation of a new approximation to (5)

Despite good performance near $\theta_c = 0$, (19) can converge quite poorly for larger values of θ_c. This can be remedied in part via the use of Padé approximants, three representative examples of which are

$$F_{1,1} = \frac{72\pi - 4\left(3+\pi^2\right)\theta_c}{18\pi - \left(12+\pi^2\right)\theta_c} \approx \frac{4 - 0.910338\theta_c}{1 - 0.38674\theta_c}, \tag{21}$$

$$F_{2,2} \approx \frac{4 - 1.32178\theta_c + 0.155932\theta_c^2}{1 - 0.4896\theta_c + 0.0553538\theta_c^2}, \tag{22}$$

$$F_{3,3} \approx \frac{4 - 1.87553\theta_c + 0.347231\theta_c^2 - 0.0234791\theta_c^3}{1 - 0.628038\theta_c + 0.125212\theta_c^2 - 0.00846695\theta_c^3}. \tag{23}$$

We examine the behaviour of these approximants compared to the models (7)–(13) in Fig. 3. Despite the poor behaviour of the naïve expansion at $\theta_c = \pi^-$—which we discuss further presently—the Padé approximants perform significantly better over a wide range of θ_c. Indeed, they outperform almost all approximations until close to $\theta_c = \pi^-$.

In order to remedy the behaviour at $\theta_c = \pi^-$ by preserving the correct singular behaviour, we posit an ansatz for the integral flux based on two-point Padé approximants of the form

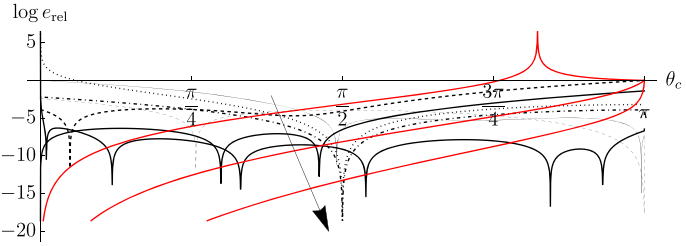

Fig. 3 Logarithmic relative error of different approximations to the exact solution (5). Black curves are existing approximations from the literature in the same line styles as in Fig. 1, while the red curves are the three Padé approximants discussed in Sect. 3, with the arrow indicating the direction of increasing order of approximation

$$F_a = \frac{a_0 + a_1\theta_c + a_2\theta_c^2}{(\pi - \theta_c)(1 + b_1\theta_c + b_2\theta_c^2)}. \tag{24}$$

The five constants are fixed by imposing the leading-order behaviour at $\theta_c = 0^+, \pi/2$ and π^-, and the first-order behaviour at $\theta_c = 0^+$ and $\theta_c = \pi^-$. This yields

$$F_a = \frac{2\pi}{(\pi - \theta_c)} \frac{\begin{array}{c}\left[-2\left(\pi + (4+\pi)\log^2(2) - \pi\log(8)\right)\theta_c^2 + \right. \\ \left. \pi(4 - 5\log 2)(\pi - 4\log 2)\theta_c + 2\pi^2(\pi - 4\log 2)(\log 2 - 1)\right]\end{array}}{\begin{array}{c}\left[\pi^2(\pi - 4\log 2)(\log 2 - 1) + \right. \\ \left. \pi(3 - 4\log 2)(\pi - 4\log 2)\theta_c/2 + \left(-4 + \pi - 4\log^2 2 + \log(16)\right)\theta_c^2\right]\end{array}} \tag{25}$$

$$\approx \frac{4\pi}{\pi - \theta_c} \cdot \frac{1 - 0.2771\,\theta_c + 0.0358\,\theta_c^2}{1 - 0.1180\,\theta_c + 0.00683\,\theta_c^2}. \tag{26}$$

Forms of these suited for import into Mathematica are given in Appendix A. Both (25) and (26) are in absolute error compared to the exact solution (5) by $\lesssim 0.05\%$ across the entire range of contact angles, while also retaining the desired asymptotic properties at $\theta_c = 0^+, \pi/2$ and π^-. These approximations are compared to the existing models discussed in Sect. 1 in Fig. 4.

The approximation (25) generally gives substantially better agreement with the exact answer, other than at isolated values of θ_c, where (6) is superior. Indeed, despite somewhat awkwardly being composed of two functions for different ranges of θ_c, the approximations of [17] hold up very well, with the only substantial differences in the superhydrophobic limit, $\theta_c = \pi^-$ and in the gradient $F'(\theta_c)$ in the hydrophilic limit, $\theta_c = 0^+$.

4 Performance in key asymptotic limits

The asymptotic behaviour of solutions in certain limits is of significant theoretical and practical interest. In particular, even seemingly small quantitative errors can prove critical in limits, where the flux becomes large (e.g. $\theta_c \to \pi^-$) and the resultant abso-

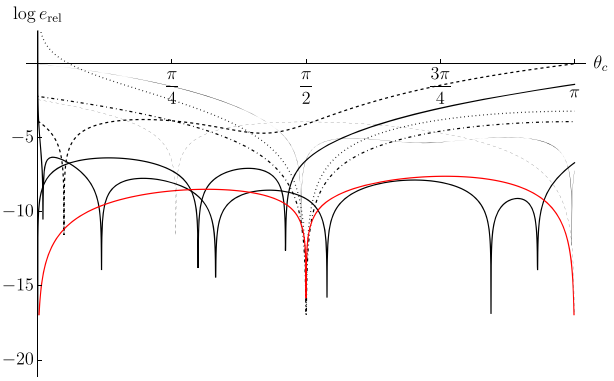

Fig. 4 Logarithmic relative error of different approximations to the exact solution (5). Black curves are existing approximations from the literature in the same line styles as in Fig. 1, while the red curve corresponds to the approximation (25)

Table 1 A comparison of the asymptotic behaviours of the various models at key contact angles: the hydrophilic limit $\theta_c = 0^+$, the hemispherical droplet $\theta_c = \pi/2$ and the superhydrophobic limit $\theta_c = \pi^-$

	Model	$F(\theta_c = 0^+)$	$F'(\theta_c = 0^+)$	$F(\theta_c = \pi/2)$	$F'(\theta_c = \pi/2)$	$\lim_{\theta_c \to \pi^-} (\pi - \theta_c) F(\theta_c)$	$\lim_{\theta_c \to \pi^-} \partial_{\theta_c}[(\pi - \theta_c) F(\theta_c)]$
	Exact	4	$2/\pi$	2π	π	$4\pi \log 2$	0
∞	$F_{\text{p,thin}}$	4	0.603	6.27	3.04	6.54	-3.64
∞	$F_{\text{p,thick}}$	$0.00056\theta_c^{-1}$	$-0.00056\theta_c^{-2}$	6.28	3.15	8.72	0.09
∞	F_{bour}	$\frac{-2\pi}{\theta_c \log \theta_c^2/2}$	$\frac{2\pi}{\theta_c^2 \log \theta_c^2/2}$	2π	π	$2\pi/\log 2$	0
∞	F_{hula}	4.08	0	6.18	2.66	0	−12.5
∞	F_{huwu}	$\sqrt{2}\pi$	0	2π	π	$2\sqrt{2}\pi$	0
∞	F_{bhar}	0	5.195	6.29	3.45	8.70	−0.407
∞	F_{lest}	$2\pi \log 2$	0	$2\sqrt{2}\pi \log 2$	$\sqrt{2}\pi \log 2$	$4\pi \log 2$	0
∞	(25)	4	$2/\pi$	2π	3.15	$4\pi \log 2$	0

Dark shading corresponds to exact agreement with the true asymptotic value, while light shading indicates numerical agreement to within 1%

lute error can be substantial. Qualitative errors, such as incorrect scaling behaviours in relevant limits, can mean that models are inappropriate even in the coarsest approximations. We therefore explore the accuracy of all the approximate solutions discussed herein in more detail in Table 1. In particular, we compare the leading- and first-order behaviours at $\theta_c = 0, \pi/2$ and π to the exact value. Dark shaded boxes correspond to exact agreement, while light shaded boxes correspond to numerical agreement within 1%.

In general, the models that exhibit the strongest agreement numerically across the full range (see, for example, the model of [17] F_{pick} (6)) exhibit the weakest asymptotic properties, and vice versa (see, for example, the model of [21] F_{lest} (13)). The model (25) exhibits exact agreement in all limits except first-order behaviour at $\theta_c = \pi/2$; even in this latter case, the error is within 1%. Thus, there is a strong indication that its use may be acceptable even in asymptotic calculations for $\theta_c \approx \pi/2$, where accuracy may be critical.

5 Applications

While there are multiple applications of the integral flux and, thus, the new approximation (25), we illustrate its accuracy and asymptotic veracity for two particular example applications. The first is an example that has practical considerations, but for which calculation using the exact solution (5) is somewhat cumbersome, namely calculation of droplet lifetimes in Sect.5.1, and the second is the calculation of the local flux J in Sect.5.2.

5.1 Application to droplet lifetimes

We aim to reproduce the droplet lifetime results of [9] without using numerical quadrature. These results give the extinction time of an evaporating droplet in three critical regimes: a constant contact radius droplet (CR), corresponding to a pinned contact line; a constant contact angle droplet (CA), corresponding to a sliding contact line; and a combination stick–slip droplet (SS), where the current mode depends on the current contact angle and the value of the receding contact angle. We introduce the notation θ_0 to denote the initial contact angle, and θ^* to denote the angle at which the droplet switches from CR to CA behaviour when evaporating in the SS mode. The stick–slip mode is particularly cumbersome using the exact solution (5), but becomes a triviality with the new approximation (25).

To this end, we define the function

$$g(\theta_c) = \frac{(1+\cos\theta_c)^2 F(\theta_c)}{\pi R} \tag{27}$$

so as to coincide with that defined in Eq. (2.2) of [9]. With (25) available this is of course simple to write down. However, the integrals to be computed are analytically challenging due to the mix of rational and trigonometric functions. We therefore use a simple rational polynomial approximation

$$(1+\cos\theta_c)^2 \approx \frac{0.0410637+0.0355073\theta_c+0.00719019\theta_c^2}{1-0.408889\theta_c+0.184809\theta_c^2-0.0390888\theta_c^3+0.00580674\theta_c^4} \times(\pi-\theta_c)^4, \tag{28}$$

which is accurate up to a relative absolute error of approximately 0.004%. The integrals then become analytically tractable.

Following the notation above, the droplet lifetimes t_i in the three modes $i =$ CR, CA, SS are given by [9]

$$t_{CR} = \left(\frac{2(1+\cos\theta_0)^2}{\sin\theta_0(2+\cos\theta_0)}\right)^{2/3} \int_0^{\theta_0} \frac{2\,\mathrm{d}\theta}{g(\theta)}, \tag{29}$$

$$t_{CA} = \left(\frac{2(1+\cos\theta_0)^2}{\sin\theta_0(2+\cos\theta_0)}\right)^{2/3} \frac{\sin\theta_0(2+\cos\theta_0)}{g(\theta_0)}, \tag{30}$$

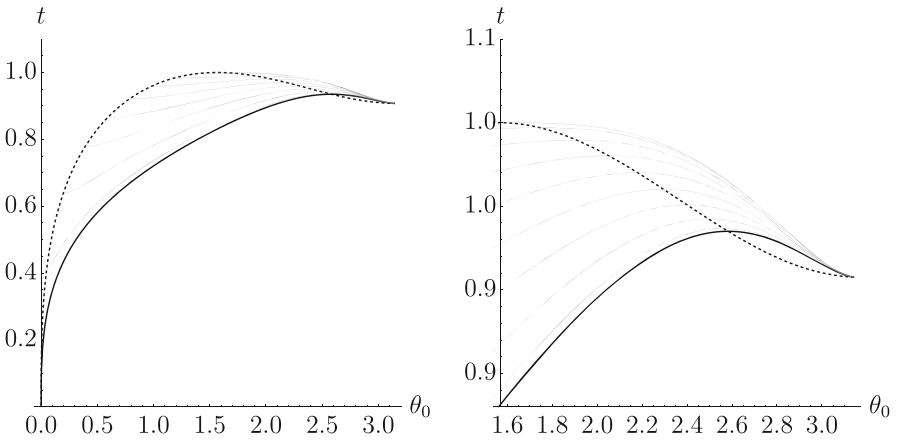

Fig. 5 An illustration of the accuracy and utility of our approximation (25), where we recreate figure 3 of [9]. The lifetime of a droplet evaporating in the SS mode, t_{SS} is plotted as a function of the initial contact angle θ_0 for $\theta^* \in \{\pi/64, \pi/16, \pi/8, 3\pi/16, \pi/4, 5\pi/16, 3\pi/8, 7\pi/17, \pi/2\}$ together with the CA and CR lifetimes t_{CA} and t_{CR} plotted as the thick dashed and solid lines, respectively

$$t_{SS} = \left(\frac{2(1+\cos\theta_0)^2}{\sin\theta_0(2+\cos\theta_0)}\right)^{2/3}\left[\int_{\theta^*}^{\theta_0}\frac{2\,\mathrm{d}\theta}{g(\theta)} + \frac{\sin\theta^*(2+\cos\theta^*)}{g(\theta^*)}\right], \tag{31}$$

where the integrals may be computed explicitly using the forms (25) and (28) in (27). The results, as shown in Fig. 5, are indistinguishable from those shown in [9] but have required no numerical quadrature at any stage.

In addition to the computational advantages, the approximation (25) has distinct advantages over the existing approximations in the literature introduced in Sect. 1. Indeed, while some suffer from a lack of accuracy, with some at best in error by a few percent (e.g. [21]), others suffer from having incorrect asymptotic properties in particular limits, with worst-case scenarios leading to non-integrable singularities (e.g. [20]).

We note that the next best accuracy for lifetimes is given by (8) [17], the results of which are indistinguishable from those given in Fig. 5. This is perhaps surprising given the divergence of the integral flux in the small contact angle limit, where $F_{p,thick} \sim \theta_c^{-1}$. However, in this approximation, the convergence of the droplet lifetimes to zero as $\theta_c \to 0^+$ is so rapid that this divergence is obscured in a lifetime plot.

5.2 Application to approximate local flux

An additional application of (25) is to determine a suitable approximate form for the local flux $J(r)$. In particular, the well-known form of the singularity at the contact line [6] suggests a flux of the form

$$J(r) \propto (1-r^2)^{-\frac{\pi-2\theta_c}{2\pi-2\theta_c}}. \tag{32}$$

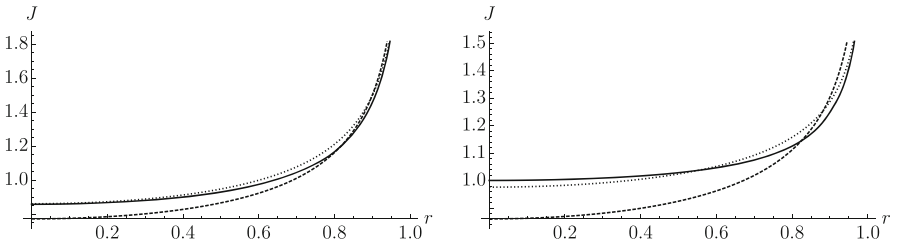

Fig. 6 A comparison of the local flux J as predicted by the exact solution (solid line), J_1 ((34), dashed line) and J_2 ((36), dotted line) for (a) $\theta_c = \pi/6$, (b) $\theta_c = \pi/3$

Access to (25) gives a suitable way to determine the constant of proportionality; in particular, we set

$$J_1(r) = F_a \frac{(1-r^2)^{-\frac{\pi-2\theta_c}{2\pi-2\theta_c}}}{\int_0^1 \int_0^{2\pi} (1-r^2)^{-\frac{\pi-2\theta_c}{2\pi-2\theta_c}} r\sqrt{1+h_r^2}\,\mathrm{d}\theta\,\mathrm{d}r} \tag{33}$$

$$= F_a \frac{(1-r^2)^{-\frac{\pi-2\theta_c}{2\pi-2\theta_c}}}{2\,(\pi-\theta_c)\;{}_2F_1\left(\frac{1}{2},\,1;\,1+\frac{\pi}{2\pi-2\theta_c};\,\sin^2(\theta_c)\right)}, \tag{34}$$

where the dimensionless form of (1) is

$$h = \sqrt{\mathrm{cosec}^2\,\theta_c - r^2} - \cot\theta_c, \tag{35}$$

F_a is as given in (25) and ${}_2F_1$ is the hypergeometric function. This is exact at $\theta_c = 0$ and $\theta_c = \pi/2$ and retains both the correct integral flux (to within 0.05%) as well as the correct singularity away from the contact line. In addition, comparison with the numerical form due to [1] reveals that the formula is never in error by more than 14.4%.

However, this can be improved by using the approximation of [7], who showed via fitting to FEM results that, for a flux of the form $J \propto (1-r^2)^{-\lambda}$, a more suitable value of λ in the bulk of the droplet is $\lambda = 1/2 - \theta_c/\pi$. Using this form, we instead find

$$J_2(r) = F_a \frac{(1-r^2)^{1/2-\theta_c/\pi}(\pi+2\theta_c)}{2\pi^2\,{}_2F_1\left(\frac{1}{2},\,1;\,\frac{\theta_c}{\pi}+\frac{3}{2};\,\sin^2(\theta_c)\right)}. \tag{36}$$

While this will have a diverging difference from the exact solution at the contact line, it has an error of at most 4% for $0 \le r \le 0.8, 0 \le \theta_c \le \pi/2$ (compared to 14% for (34)). As expected, J_2 (36) performs quite well in the bulk of the domain and, despite the inaccuracy in its singularity, may prove helpful for approximate formulations. While there are numerous possible options to improve agreement with the exact solution—such as using a composite of (34) and (36)—these are beyond the scope of the present note.

6 Conclusions

In this note, a new approximation (25) has been presented for the integral flux for a volatile droplet evaporating diffusively into the surrounding gas. This approximation is a simple rational function, which affords it significant computational benefits over the cumbersome exact solution (5), while having the advantage over previous iterations in the literature due to retaining the correct asymptotic behaviour in three key regimes: hydrophilic droplets ($\theta_c \to 0^+$); hemispherical droplets ($\theta_c = \pi/2$); and superhydrophobic droplets ($\theta_c = \pi^-$).

The resulting form is highly robust and suffers from no singularities or spurious blow-ups across the whole range of possible contact angles and is highly accurate, exhibiting errors of no more than 0.05% across the whole domain. It is more accurate than all known previous approximations aside from near a handful of isolated points and, as stressed above, unlike previous approximations, retains the correct asymptotic behaviour in key regimes.

The applications of this approximation extend beyond droplet evaporation. Since the integral flux (5) is found by solving a classical mixed boundary value problem for Laplace's equation, there are analogues in multiple other physical fields, such as the capacitance of a hemispherical cap in electrostatics [23] or the growth rate of ice crystals [24]. We anticipate similar benefits in terms of computational speed combined with asymptotic accuracy in such applications.

Acknowledgements MRM would like to acknowledge the support of EPSRC Grant EP/X035646/1. The authors would like to thank the reviewers, whose comments helped improve a previous version of this manuscript.

Appendix A: Mathematica form of fluxes

Here we give the present approximations (25) and (26) in a Mathematica-friendly form for people wishing to use this in applications. For ease of use, we use x as notation for the droplet contact angle.

```
asymptoticFlux=Uncompress["1:eJzVUs0OgjAMRhnGo6/g+\
3ggxBfAhJkl6BKn0XeXoLRlkW4VDDc5ENp9fyvdHmyh0yRJXNa
99uZUOb30ZW7v1YVKBWV\
9cw6q3HwwSDGv7nGLrnzgJyl6TgiGvtdR/\
AiRqMNtkRPqPMEJwA7sdvaI9NH4lC7iUHvF5RvocbE+NcGDI7r9
ZIIvA2xGcs2+\
UDptLIw5ApJt7IF35btDi9ALMMZaGAzLZwCuMyEdUIvyauy5rBElTXn
```

```
4a8QNSoUNkqc+f+\
BS+ihh+x/LoxiyGfxXyf23ZWHtjbd6A9t0Gfk="];

approximateFlux=ToExpression[
"\\frac{4\\pi}{\\pi-x}
        \\frac{1-0.2771 x+ 0.0358x^2}
            {1-0.1180 x+0.00683x ^2}",TeXForm,HoldForm];
```

References

1. Popov YO (2005) Evaporative deposition patterns: spatial dimensions of the deposit. Phys Rev E 71(3):036313
2. Murisic N, Kondic L (2011) On evaporation of sessile drops with moving contact lines. J Fluid Mech 679:219–246
3. Shahidzadeh-Bonn N, Rafai S, Azouni A, Bonn D (2006) Evaporating droplets. J Fluid Mech 549:307–313
4. Kelly-Zion P, Pursell C, Vaidya S, Batra J (2011) Evaporation of sessile drops under combined diffusion and natural convection. Colloids Surf A 381(1–3):31–36
5. Dollet B, Boulogne F (2017) Natural convection above circular disks of evaporating liquids. Phys Rev Fluids 2(5):053501
6. Deegan RD, Bakajin O, Dupont TF, Huber G, Nagel SR, Witten TA (1997) Capillary flow as the cause of ring stains from dried liquid drops. Nature 389(6653):827–829
7. Hu H, Larson RG (2002) Evaporation of a sessile droplet on a substrate. J Phys Chem B 106(6):1334–1344
8. Wilson SK, D'Ambrosio H-M (2023) Evaporation of sessile droplets. Annu Rev Fluid Mech 55:481–509
9. Stauber JM, Wilson SK, Duffy BR, Sefiane K (2014) On the lifetimes of evaporating droplets. J Fluid Mech 744:2
10. Malinowski R, Volpe G, Parkin IP, Volpe G (2018) Dynamic control of particle deposition in evaporating droplets by an external point source of vapor. J Phys Chem Lett 9(3):659–664
11. Brondi C, Di Novo NG, Pugno NM, Mensitieri G, Fraldi M (2023) Prediction of virus survival timescales in surrogate respiratory sessile droplets. Phys Fluids 35(5):057109
12. Fabrikant V (1987) Diffusion through perforated membranes. J Appl Phys 61(3):813–816
13. Wray AW, Moore MR (2023) Evaporation of non-circular droplets. J Fluid Mech 961:11
14. Weber H (1873) Über die Besselschen Functionen und ihre Anwendung auf die Theorie der elektrischen Ströme. J Reine Angew Math 76(1):75–105
15. Lebedev NN, Silverman RA, Livhtenberg D (1972) Special functions and their applications. Dover, Mineola
16. Virey EH, Baron N, Bouhamri Z (2020) 30-4: microled display technology trends and intellectual property landscape. In: SID symposium digest of technical papers, vol 51, pp 436–439. Wiley Online Library
17. Picknett R, Bexon R (1977) The evaporation of sessile or pendant drops in still air. J Colloid Interface Sci 61(2):336–350
18. Bourges-Monnier C, Shanahan M (1995) Influence of evaporation on contact angle. Langmuir 11(7):2820–2829
19. Hu D, Wu H, Liu Z (2014) Effect of liquid-vapor interface area on the evaporation rate of small sessile droplets. Int J Therm Sci 84:300–308
20. Bhardwaj R (2018) Analysis of an evaporating sessile droplet on a non-wetted surface. Colloid Interface Sci Commun 24:49–53
21. Lebedev-Stepanov P, Savenko O (2023) Evaporation of small sessile drop deposited on horizontal solid surface: new exact solutions and approximations
22. Larsson C, Kumar S (2022) Quantitative analysis of the vertical-averaging approximation for evaporating thin liquid films. Phys Rev Fluids 7(9):094002

23. Ciftja O (2021) Electrostatic potential energy stored in a hemispherical surface with uniform surface charge distribution. J Electrostat 111:103579
24. McDonald JE (1963) Use of the electrostatic analogy in studies of ice crystal growth. Z Angew Math Phys ZAMP 14:610–620